Available online at www.sciencedirect.com
ScienceDirect
Journal of Power Sources 162 (2006) 9–20
JOURNAL OF POWER SOURCES
www.elsevier.com/locate/jpowsour

Sol–gel-modified boron-doped diamond surfaces for methanol and ethanol electro-oxidation in acid medium

G.R. Salazar-Banda, H.B. Suffredini, M.L. Calegaro, S.T. Tanimoto, L.A. Avaca *

Instituto de Química de São Carlos, Universidade de São Paulo, C.P. 780, 13560-970, São Carlos-SP, Brazil

Received 18 May 2006; accepted 15 June 2006
Available online 25 July 2006

Abstract

Studies of the methanol and ethanol electro-oxidation reactions on boron-doped diamond (BDD) electrode surfaces modified with Pt, Pt-RuO_2 and Pt-RuO_2-RhO_2 by the sol–gel method are reported here. The materials were initially characterized by X-ray diffraction (XRD), atomic force microscopy (AFM), scanning electron microscopy (SEM) and energy dispersive X-ray analysis (EDX). The XRD analyses indicate that the sol–gel method produces nano-sized deposits on the BDD surfaces. These deposits also form nano-clusters with a size of ca. 100 nm as observed by SEM and AFM. The EDX maps showed that the metals are homogeneously distributed on the BDD surface and have a composition close to the expected one. Cyclic voltammetry experiments in acid medium revealed that the CO poisoning effect for the methanol and the ethanol oxidation reactions is largely inhibited on the Pt-RuO_2-RhO_2/BDD electrode showing the positive contribution of the rhodium oxide to the electrocatalysts performance in these reactions. Potentiostatic polarization curves and the corresponding Tafel plots showed that the addition of RuO_2 and RhO_2 to Pt/BDD produces a more reactive electrocatalyst that adsorbs methanol and ethanol more efficiently and changes the reactions onsets by 120 or 180 mV towards less positive potentials, respectively. Moreover, the stationary current density measured at a fixed potential for ethanol oxidation on the Pt-RuO_2-RhO_2/BDD composite electrode is more than one order of magnitude larger than on a Pt/BDD surface. In addition, chronoamperometric experiments indicate that on those composite electrodes the effect of CO poisoning only appears after a considerable amount of charge has passed through the interface. Consequently, the catalyst containing Pt, RuO_2 and RhO_2 deposited on BDD by the sol–gel method is a very promising composite material to be used in fuel cell anodes.

Keywords: Modified boron-doped diamond; Methanol oxidation; Ethanol oxidation; Sol–gel method

1. Introduction

The need for more efficient energy conversion systems is presently in great evidence as the world fossil fuel sources become depleted as well as by the need of reducing the pollution in large urban centers. Fuel cells have proved to be an interesting and very promising alternative to solve the problem of clean electric power generation with high efficiency [1]. Methanol has been considered an interesting alternative to hydrogen for fuel cell applications since it is a liquid at room temperature thus making handling and storage much easier than in the case of hydrogen. Ethanol has similar features to those of methanol and is less toxic and easily obtained from fermentation processes of agricultural crops thus avoiding the increase of CO_2 in the atmosphere. In addition, the permeability of ethanol through Nafion® membranes is much lower than methanol [2], preventing the crossover of the fuel that causes depolarization of the cathode. Meanwhile, the complete electrochemical oxidation of ethanol to carbon dioxide is more difficult to achieve than for methanol oxidation.

At room or moderate temperature, the use of pure platinum as a catalyst for ethanol or methanol electro-oxidation is not very appropriate because it is readily poisoned by strongly adsorbed intermediates. It has been shown that the combination of Pt with a second or a third component is a convenient way to modify the electrocatalytic properties of this metal [3]. Metals like Ru [4–7], Sn [5,8–10] and Mo [11] have been successfully used for this purpose.

Very interesting results have been observed on Pt-Ru catalysts and it has been proposed that the Ru atoms activates water

* Corresponding author. Tel.: +55 16 3373 9943; fax: +55 16 3373 9943.
E-mail address: avaca@iqsc.usp.br (L.A. Avaca).

0378-7753/$ – see front matter © 2006 Elsevier B.V. All rights reserved.
doi:10.1016/j.jpowsour.2006.06.045

molecules and provide preferential sites for OH_{ads} adsorption at lower potentials than Pt. Abundant $–OH_{ads}$ species are necessary to completely oxidize to CO_2 the poisoning intermediates. This process is known as the bifunctional mechanism [12] and is one of the most accepted to explain the synergistic effect observed on Pt-Ru alloys used as catalysts for the electro-oxidation of methanol [13,14]. Some authors have also proposed that Ru enhances methanol oxidation through an electronic effect on neighboring Pt atoms (the ligand effect) [15,16]. In this mechanism, it has been proposed that Ru may accelerate the adsorption and dehydrogenation of methanol on Pt sites at low potentials or, alternatively, it may weaken the Pt–CO bond allowing the oxidation of CO at lower potentials.

The multifunctional requirements of a catalyst for the direct oxidation of small organic molecules include the ability to activate C–H, C–O and even C–C bonds suggesting that an optimum performance will require a binary, ternary or even quaternary catalyst [13]. In this sense, de Souza et al. [17] have demonstrated that metallic Rh used in combination with Pt can increases the activity for ethanol C–C bond dissociation. This feature is very interesting when the aim is the ethanol electrooxidation but is not enough to produce a good electrocatalyst since Rh does not help in decrease significantly the energy barrier for CO oxidation. On the other hand, the addition of Ru could help by decreasing the energy of the CO–Pt bond and also by diminishing the activation energy for the dehydrogenation process. Thus, a good electrocatalyst for this reaction would probably need the presence of rhodium and ruthenium to improve simultaneously the dehydrogenation of ethanol, the C–C bond dissociation and the decrease of the Pt–CO bond strength.

Recently, Jayaraman and Hillier [18] studied the reactivity towards the oxidation of hydrogen, carbon monoxide, methanol and ethanol on ternary $Pt_xRu_yRh_z$ metallic electrodes using the combinatorial method and concluded that the best composition range for lowering the onset oxidation overpotentials is $25\% < Pt < 50\%$, $20\% < Ru < 50\%$ and $10\% < Rh < 50\%$. To the best of our knowledge, no other investigations have been carried out focusing the methanol or ethanol oxidation on Pt-Ru-Rh ternary catalysts.

The long-term stability of the membrane–electrode-assembly (MEA) in polymer electrolyte membrane fuel cells (PEMFCs) is a matter of great concern due to the degradation the of components in either oxidizing or reducing environments accompanied with the electrode potentials induced by the cell reaction [19–21]. Typical sp^2-bonded carbon with high surface area is the most often used support material in fuel cells systems and it is susceptible to micro structural and morphological degradation under oxidizing conditions [22]. One particular concern is its electrochemical instability particularly under corrosive and/or oxidative conditions [23–26]. Degradation of the carbon support is a serious technological problem since it leads to either a loss of electrocatalytic activity due to catalyst detachment, aggregation of the particles or general mechanical failure of the electrodes. This effects can increase the ohmic resistance and therefore reduce the operational efficiency of PEMFCs [20–22,27,28].

The development of advanced supporting materials that are more stable at relatively high temperatures (150–200 °C) without suffering micro-structural or morphological degradation in aggressive chemical environments is highly desirable [22]. Boron-doped conductive diamond materials mainly composed of sp^3 type carbon appear as a feasible alternative to be used for supporting the catalysts.

Boron doped diamond (BDD) electrodes have been extensively used in recent years either in fundamental studies of their electrochemical properties [29–34] as well as in technological applications. These materials have high chemical and thermal stability, extreme hardness and strong corrosion resistance [35,36]. Moreover, they are chemically inert and have a very low capacitive background current. All these properties made BDD electrodes very attractive for their use in electrosynthesis [37,38], electroanalysis [39–44], electrochemical combustion of unwanted compounds [45–50] as well as a conductive support in electrocatalysis [52–56].

Recently, Fischer and Swain [51] reported the production of electrically conducting diamond powder prepared by coating insulating diamond powder (8–12 μm diameter, $\sim 2\ m^2\ g^{-1}$) with a thin boron-doped layer using microwave plasma-assisted chemical vapor deposition and suggested the use of this advanced carbon material as a new dimensionally stable electrocatalyst support. In fact, the future of advanced anodes for direct-alcohol fuel cell systems should be focused on the use of this new material.

The first study showing the possibility of the electrochemical deposition of Pt, Pb and Hg adlayers on BDD surfaces was reported by Awada et al. [52]. Methanol oxidation was studied by Montilla et al. [53] on a Pt-modified diamond electrode where the platinum particles were deposited on the BDD surface by conventional chemical or electrochemical methods. The stability of the deposited Pt was low showing a loss of 65% of the initial Pt particles after cycling the potential between the water decomposition reactions. Nevertheless, the activity for methanol oxidation was satisfactory. Honda et al. [56] studied the electrocatalytic activity for oxygen reduction and methanol oxidation of a boron-doped nanoporous honeycomb diamond films modified with Pt nanoparticles. The Pt particles were deposited by immersion of the BDD electrodes in a H_2PtCl_6 aqueous solution and subsequent reduction in a heated H_2 atmosphere. These deposits also showed a very low stability.

Previous work from this laboratory by Salazar-Banda et al. [54] has shown great improvements in the stability of Pt particles deposited on the BBD surface by the sol–gel method by using a thermal pre-treatment. This procedure yielded electrodes that retained over 90% of the coated material after 1000 voltammetric cycles carried out between the water decomposition reactions. Moreover, covering the modified electrode surface with a Nafion® film made negligible the clusters detachment/dissolution. In another work that used a similar electrode (Pt/BBD + Nafion® film), Suffredini et al. [55] showed that 1000 voltammetric cycles for the ethanol oxidation also left the surface practically unchanged. In addition, preliminary studies for the ethanol oxidation reaction on Pt/BDD and Pt-RuO_2/BDD

electrodes demonstrated the excellent catalytic activity of the mixed sol–gel coating.

It is well established in literature that the sol–gel method is an excellent alternative for producing stable coatings on different surfaces and it has been used for different purposes, such as the construction of sensors [57] and corrosion protection [58] among others. While carbon powder electrodes were modified by the same method and the resulting materials were used as anodes for the direct oxidation of methanol using a Nafion® suspension to fix the Pt-RuO_2/C composite onto a glassy carbon support [7].

The aim of this work is to use of the sol–gel method to generate Pt, Pt-RuO_2 and Pt-RuO_2-RhO_2 deposits on BDD electrode surfaces for the oxidation of methanol and ethanol. The composite coatings will be physically characterized by X-ray diffraction (XRD), atomic force microscopy (AFM), scanning electron microscopy (SEM) and energy dispersive X-ray (EDX) analyses. In the sequence, studies of the electro-oxidation of methanol and ethanol in acid media will be carried out using different electrochemical techniques such as cyclic voltammetry, steady-state polarization curves, Tafel plots and chronoamperometry.

2. Experimental

Boron-doped diamond (BDD) electrodes were prepared in the Centre Suisse d'Electronique et de Microtechnique SA (CSEM), Neuchâtel, Switzerland, using the hot filament chemical vapor deposition (HF-CVD) technique with a filament temperature in the range of 2440–2560 °C and a gaseous mixture containing methane, H_2 and trimethylboron, having a final boron content of the order of 800 ppm. BDD plates (1.2 cm × 1.2 cm) were used as working electrode and as substrate for the deposition of the catalysts.

The reagents used in this work were Merck P.A. quality and water was purified by the Milli-Q system from Millipore. The sol–gel solutions were prepared with Pt(II), Ru(III) and Rh(III) acetylacetonates in a mixture of isopropyl alcohol + acetic acid (3:2, v/v), following published routines [54,55,59,60]. The final concentration of each of these solutions was 0.01 mol L^{-1}.

The preparation of the Pt, Pt-RuO_2 and Pt-RuO_2-RhO_2 coatings using the sol–gel method was carried out onto the BDD surfaces after a previous thermal pre-treatment at 400 °C for 30 min in air. A mixed solution of the Pt(II), Ru(III) and/or Rh(III) acetylacetonates with the desired composition was transferred to the diamond surface by the painting technique. After that, the solution was evaporated for 5 min at 80 °C in an oven. This procedure was repeated 15 times and at the end the electrodes were subjected to a thermal densification treatment at 400 °C for 1 h in an argon atmosphere.

Electrochemical experiments were carried out in a one-compartment Pyrex® glass cell provided with three electrodes and degassing facilities for bubbling N_2. The working electrode was placed in a Teflon® holder leaving an exposed circular area of 0.63 cm^2. The reference system was the hydrogen electrode in the same solution (HESS) and was connected by a Luggin capillary. The auxiliary electrode was a 2 cm^2 Pt foil. All solutions were deoxygenated by bubbling N_2 for 10 min prior to measurements.

Comparative cyclic voltammetries to determine the electrochemical active areas of the modified BDD electrodes were performed in a 1.0×10^{-2} mol L^{-1} $K_4Fe(CN)_6$ + 0.5 mol L^{-1} H_2SO_4 solution using a 0.18 cm^2 Pt disk electrode polished with $\phi = 0.25$ μm alumina powder suspension. Other electrochemical measurements were performed in either a 0.5 mol L^{-1} H_2SO_4 solution or in 0.5 mol L^{-1} H_2SO_4 + 0.5 mol L^{-1} methanol or ethanol solutions using a Model 283 EG&G PARC electrochemical instrument.

The atomic ratio of the electrocatalyst on the BDD surface was determined by energy dispersive X-ray analysis coupled to a scanning electron microscope LEO Mod. 440 with a silicon-lithium detector and a Be window and applying 113 eV. The scanning electron microscopy images were obtained with the same equipment. The surface topology studies were carried out in an atomic force microscope TopoMetrix® AFM Explorer. X-ray diffractograms of the electrocatalysts were obtained in a universal diffractometer Carl Zeiss-Jena, URD-6, operating with Cu Kα radiation (λ = 0.15406 nm) generated at 50 kV and 100 mA.

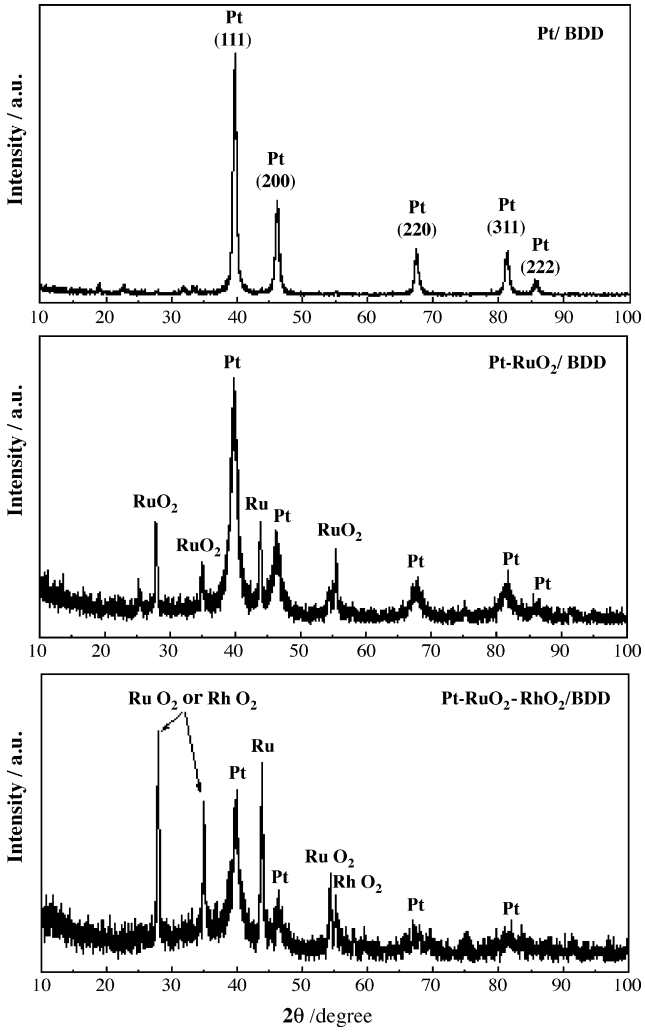

Fig. 1. Small angle XRD diffractograms of the Pt/BDD, Pt-RuO_2/BDD and Pt-RuO_2-RhO_2/BDD composite electrodes.

Scans were carried out at 1° min^{-1} for 2θ values between 5° and 100°.

3. Results and discussion

3.1. XRD analysis

Fig. 1 shows the XRD patterns obtained by continuous scan at small angle for the different deposits. The response of the Pt/BDD electrode reveals the presence of a polycrystalline platinum deposit (JCPDS #04–0802) with the characteristic peaks in the 2θ values of 39.9°, 46.2°, 67.9°, 81.0° and 86.1°, corresponding to the reflection planes (1 1 1), (2 0 0), (2 2 0), (3 1 1) and (2 2 2), respectively. This is in agreement with previous works that observed the same 2θ values for polycrystalline Pt and Pt-Ru alloys [61] and on carbon supported Pt nanoparticles [62,63]. Although the sol–gel method using acetylacetonates could produce metal or metal oxide deposits, only pure Pt was observed in the present case.

The XRD patterns for the Pt-RuO_2/BDD sample presents all the diffraction peaks corresponding to Pt as well as additional peaks at 2θ values close to 28°, 35° and 55°. These correspond to the (1 1 0), (1 0 1) and (2 1 1) crystal planes of RuO_2 crystallized as the rutile phase [64] (JCPDS #43–1027). The diffraction peak in the 2θ value of ∼43° is probably related to the presence of small amounts of metallic ruthenium in the deposit.

Similar analyses were performed with the Pt-RuO_2-RhO_2/BDD deposit. The corresponding XRD diffractogram in Fig. 1 shows the face centered cubic crystal structure of metallic Pt, the characteristic peaks of the RuO_2 rutile phase and also those associated to RhO_2 structure (JCPDS #21–1315). It is important to note that in 28° and 35° both RuO_2 and RhO_2 have characteristics diffraction peaks. This can be clearly noticed by the enhancement in the intensities of these peaks in the Pt-RuO_2-RhO_2/BDD diffractogram when compared to that of the Pt-RuO_2/BDD deposit.

Table 1
Electrodes composition and characterization

Coating	Atomic ratio in solution	Atomic ratio on the surface* (EDX)	Particle size# from XRD (nm)
Pt	100	100	6.5
Pt-RuO_2	50:50	54:46	4.4
Pt-RuO_2-RhO_2	50:25:25	56:23:21	4.3

* Mean value after four measurements in different places of the surface.
# Mean crystallite size calculated using the WinFit 1.2 software.

The XRD diffractograms of Fig. 1 were also used to estimate the mean crystallite size of the coatings using an appropriate software (WinFit 1.2) [65] and the results are presented in Table 1. These results demonstrate that the sol–gel method is an efficient and very appropriate technique to produce nanometric catalytic deposits with the desired composition on the BDD surface.

3.2. SEM, AFM and EDX measurements

Fig. 2 shows SEM images magnified 10,000× of the as received BDD surface, the Pt/DBB, the Pt-RuO_2/BDD and the Pt-RuO_2-RhO_2/BDD electrode surfaces. These images reveal that the catalysts coatings are arranged as clusters irregularly

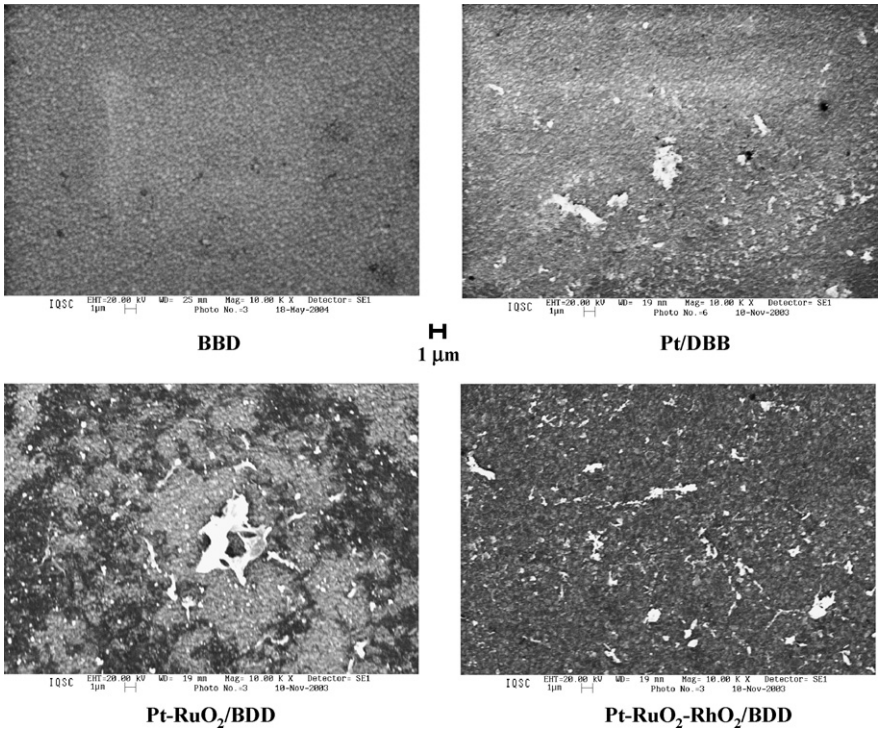

Fig. 2. SEM images recorded for the BBD, Pt/BDD, Pt-RuO_2/BDD and Pt-RuO_2-RhO_2/BDD electrode surfaces. The modified electrodes were prepared by the sol–gel method.

distributed on the DBB surface. These clusters (clear regions in figures recorded on Pt/DBB, Pt-RuO_2/BDD and Pt-RuO_2-RhO_2/BDD surfaces) seem to be composed by the agglomeration of many nanoparticles and have sizes in the range of 100 nm to 5 μm. These statements are based on EDX measurements locally performed on the referred clusters. Similar heterogeneous deposition was observed in a previous report on a BDD-PtO_x electrode surface prepared by the sol–gel method [54]. On the other hand, no deposits are detected on the bare BBD surface and only the crystalline structure of the diamond film is observed.

Fig. 3 shows the EDX composition analysis of the three catalysts studied thus confirming the presence of Pt, Ru and Rh on the BDD surface. The EDX measurements were also used to calculate the atomic proportions of the elements present in the catalytic coatings. The procedure adopted here for those calculations consisted in selecting four points in different regions of the surface and determining the composition in each one to obtain a mean value. The results are collected in Table 1 showing a very good agreement between the experimental and the expected theoretical values.

Another important aspect revealed by the EDX technique is the element map distribution shown in Fig. 4. These maps were recorded for the electrode having a Pt-RuO_2-RhO_2 coating and indicate that the catalysts particles are not only organized as clusters in the surface but also randomly and homogeneously deposited over the entire electrode with a Pt > Ru > Rh increasing content on the surface.

Fig. 5 shows the AFM topological images recorded in a 50 μm × 50 μm area for the as-received BDD surface and for the Pt/DDB, Pt-RuO_2/BDD and Pt-RuO_2-RhO_2/BDD modified electrodes. The BDD topology presents regular pyramidal structures without holes or cracks, similar to those presented in other works [66,67]. On the other hand, the modified BDD electrodes present the same general topology as before as well as the presence of small "islands" corresponding to the catalytic coatings (clear areas in the images recorded on the modified surfaces). For all BDD-modified samples, some agglomerations of the catalytic coatings can be observed and indicates the presence of heterogeneous sites with some clusters having between 1 and 5 μm and many other clusters with smaller sizes.

3.3. Electrochemical results

The electrochemical active area of the modified electrodes was roughly estimated using a previously described methodology [55]. There, the voltammetric peak current measured for the different surfaces using a typical outer-sphere and diffusion-controlled reaction as it is the case for the $K_4Fe(CN)_6/K_3Fe(CN)_6$ redox couple in solution were compared with that of a polycrystalline Pt electrode whose area was previously calculated using the H-adsorption/desorption charge density in a H_2SO_4 solution. This procedure was performed to exclude the possibility that enhanced oxidation currents could be due to surface roughness (an area effect) and not to a real catalytic effect. The voltammetric results are shown in Fig. 6 and the area values obtained are collected in Table 2. These values

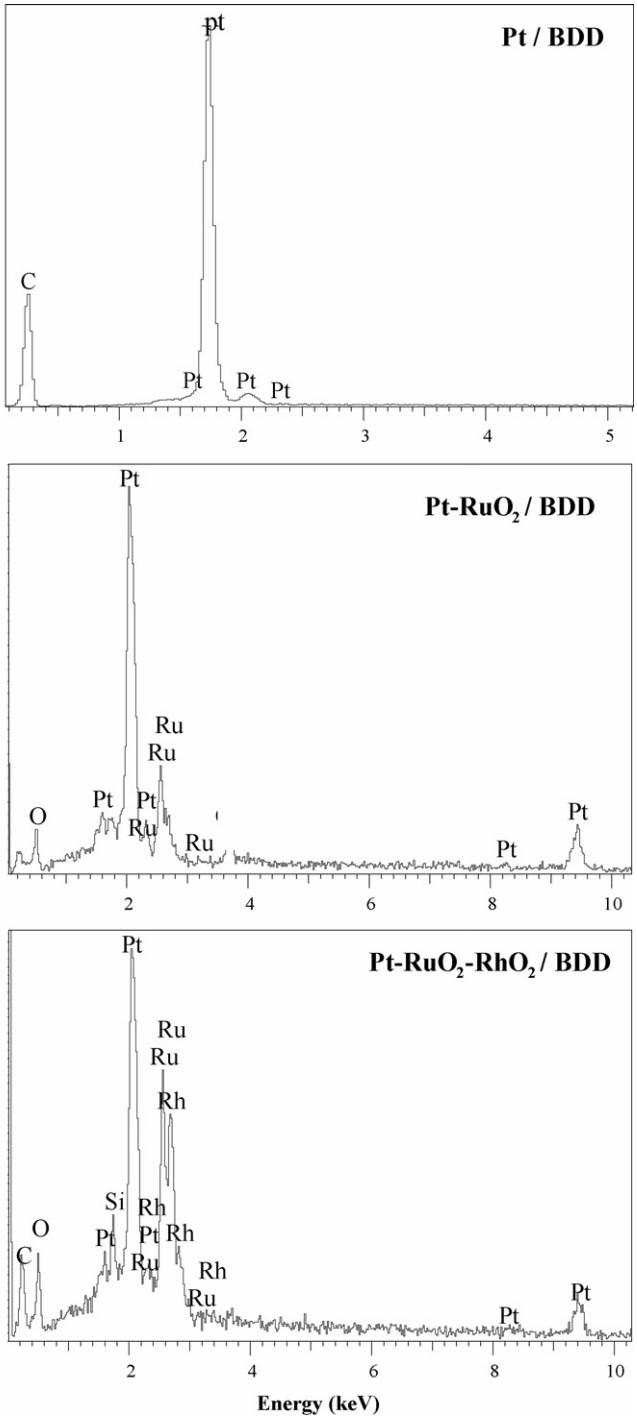

Fig. 3. EDX spectrum for Pt/BDD, Pt-RuO_2/BDD and Pt-RuO_2-RhO_2/BDD composite electrodes.

indicate that all BDD modified surfaces have an electroactive area approximately five times larger than their geometric area and that the coatings practically duplicate the original BDD area. Those area values will be later used for calculating the current densities measured for each material.

The electrochemical characterization of the electrodes was initially made by cyclic voltammetry in the supporting electrolyte (0.5 mol L^{-1} H_2SO_4 aqueous solutions). The responses are presented in Fig. 7 for BDD before (curve A) and after

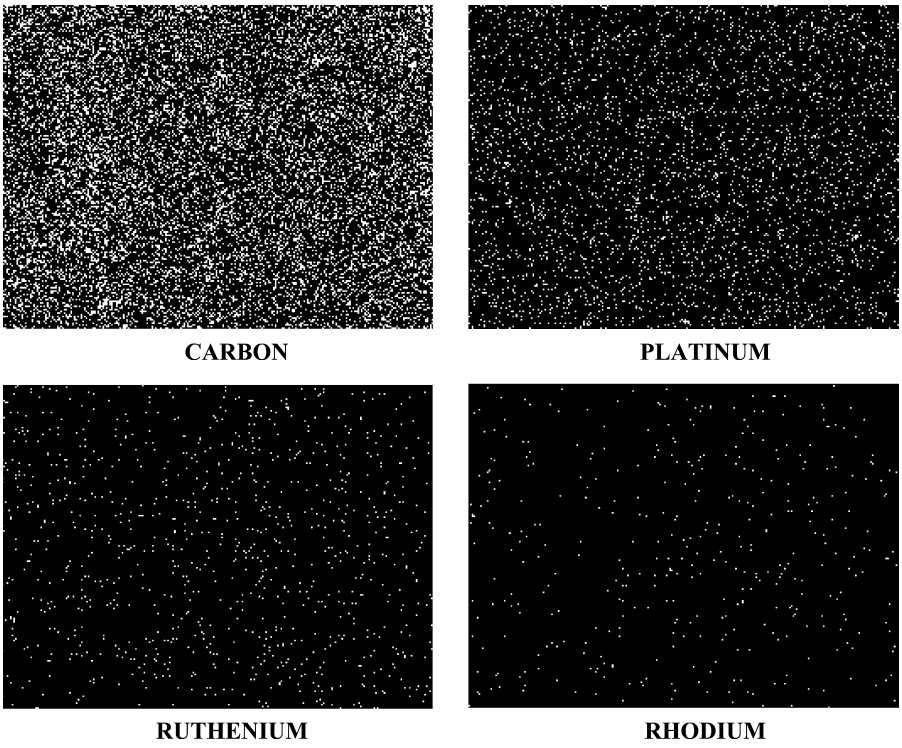

Fig. 4. EDX element's maps for the Pt-RuO_2-RhO_2/BDD electrode recorded separately in the same surface region showing the distribution of the different components.

modification with either Pt (curve B), Pt-RuO_2 (curve C) or Pt-RuO_2-RhO_2 (curve D). It is worth noticing that after modification of the BDD surface both the oxygen (OER) and the hydrogen evolution reactions (HER) are shifted towards lower potentials due to the a catalytic effect of the coatings. This is in clear contrast to the low activity of the clean BDD surface for the water decomposition, as previously reported [68]. Moreover, the curve in Fig. 7B presents the typical polycrystalline Pt surface electrochemical processes such as hydrogen adsorption/desorption and the oxide formation and reduction, demonstrating that the particles have a good electrical contact with the diamond surface and high purity.

Additionally, curve C in Fig. 7 (corresponding to the Pt-RuO_2/BDD electrode) shows inhibition of the hydrogen adsorption/desorption peaks due to the incorporation of ruthenium as well as larger currents in the double layer region due to an increase of the capacitive currents and to RuO_2 redox processes. Furthermore, the shift to lower potentials of the currents

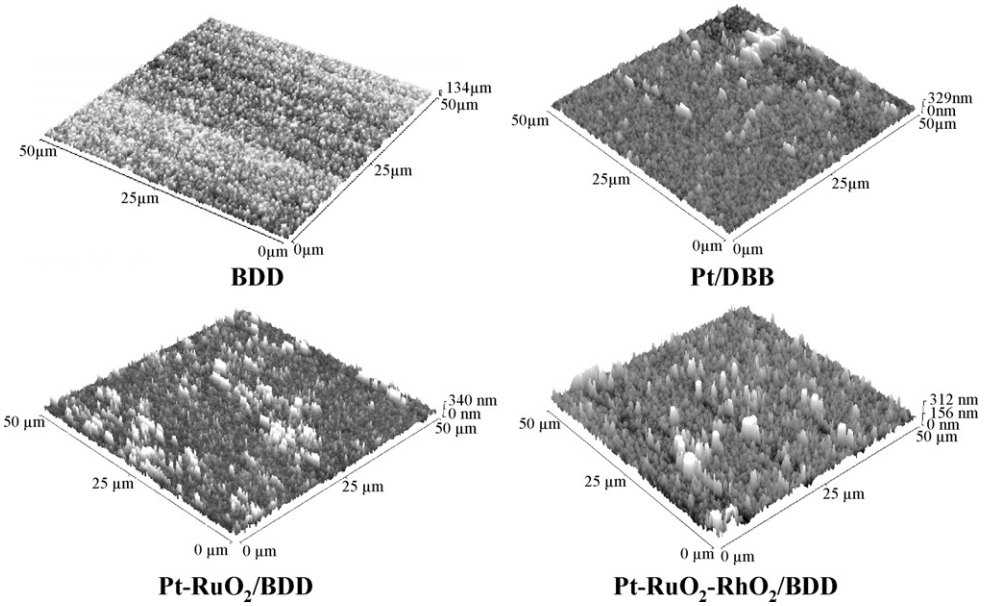

Fig. 5. Topology studies carried out by the AFM technique (50 μm × 50 μm) in the contact mode for BDD, Pt/BDD, Pt-RuO_2/BDD and Pt-RuO_2-RhO_2/BDD electrode surfaces.

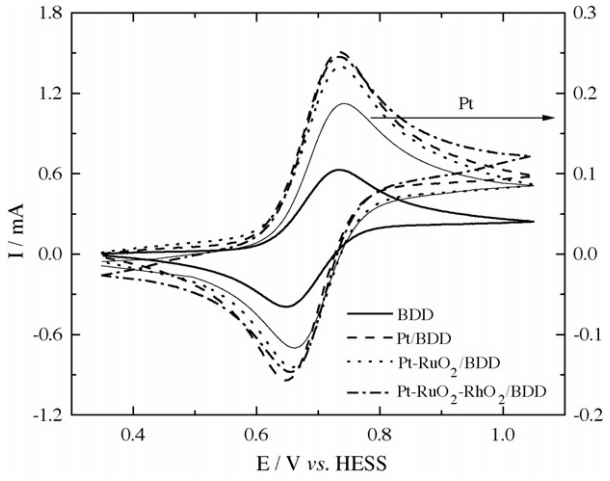

Fig. 6. Comparative cyclic voltammograms (first cycle) in a 1.0×10^{-2} mol L^{-1} $K_4Fe(CN)_6$ + 0.5 mol L^{-1} H_2SO_4 aqueous solution used to estimate the active areas of the modified electrodes ($v = 0.050$ V s^{-1}).

Table 2
Electro active areas and roughness factors obtained by comparative cyclic voltammetries with a platinum electrode in 10^{-2} mol L^{-1} $K_4Fe(CN)_6$ + 0.5 mol L^{-1} H_2SO_4

Electrode material	Geometric area (cm^2)	Electroactive area (cm^2)	Roughness factor
Polycrystalline Pt	0.18	0.32[a]	1.75
BDD	0.63	1.47	2.34
Pt/BDD	0.63	3.24	5.14
Pt-RuO_2/BDD	0.63	3.10	4.93
Pt-RuO_2-RhO_2/BDD	0.63	3.19	5.07

[a] Area determined by the hydrogen desorption charge.

associated to the oxygen evolution reaction can also be related to the presence of Ru on the BDD surface [55]. Meanwhile, curve D in Fig. 7 (corresponding to the Pt-RuO_2-RhO_2/BDD electrode) shows that the adsorbed H-layer oxidation is also inhibited in the 0.05–0.3 V region. During the negative potential sweep, the oxide reduction processes occur at more negative potentials than those observed for pure platinum and this has been attributed to the presence of rhodium in the deposit [69].

Methanol and ethanol oxidation processes in acid medium on the different electrode materials were initially studied by cyclic voltammetry at a scan rate of 0.005 V s^{-1} and are presented in Fig. 8A and B, respectively. The alcohol concentration was 0.50 mol L^{-1} and the experiments were carried out in 0.5 mol L^{-1} H_2SO_4 solutions. The solid-line curve in Fig. 8A shows that methanol oxidation has an onset potential (taken at $i = 0.1$ mA cm^{-1}) of 0.44 V versus HESS on the Pt-RuO_2-RhO_2/BDD electrode while for the Pt-RuO_2/BDD (dashed line) and the Pt/BDD (dotted-line) electrodes those potentials are ca. 0.49 and 0.60 V, respectively. Similarly, Fig. 8B shows that ethanol oxidation starts at around 0.35, 0.52 and 0.54 V versus HESS on the same materials clearly indicating the enhancement of the catalytic activity of the platinum coating in the presence of the ruthenium and rhodium oxides.

In addition, the cyclic voltammogram in Fig. 8A and B revealed that for both alcohols the reactivation currents are much lower in the whole potential range for the Pt-RuO_2-RhO_2/BDD than for the others catalyst. This could be interpreted as a more

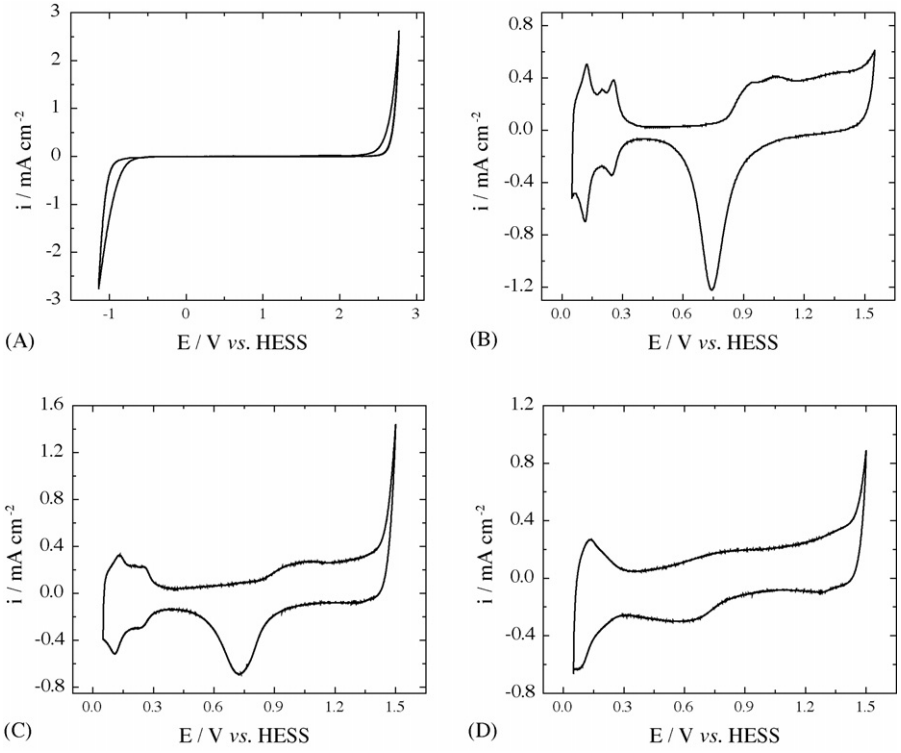

Fig. 7. Steady-state cyclic voltammograms recorded in a 0.5 mol L^{-1} H_2SO_4 aqueous solution for the BDD (A), Pt/BDD (B), Pt-RuO_2/BDD (C) and Pt-RuO_2-RhO_2/BDD (D) electrode surfaces ($v = 0.05$ V s^{-1}).

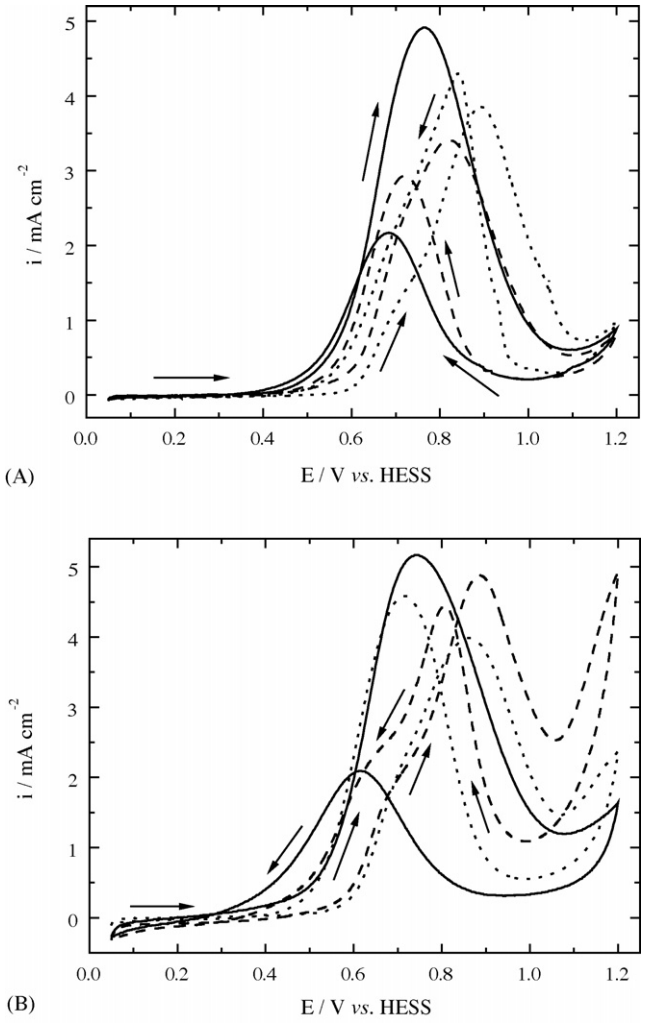

Fig. 8. Cyclic voltammograms (second cycle) for the electrochemical oxidation of 0.5 mol L^{-1} methanol (A) and 0.5 mol L^{-1} ethanol (B) dissolved in a 0.5 mol L^{-1} H_2SO_4 aqueous solution and recorded for the Pt/BDD (dotted line), Pt-RuO_2/BDD (dashed line) and Pt-RuO_2-RhO_2/BDD (solid line) electrode surfaces ($v = 0.005$ V s^{-1}).

efficient direct oxidation on the ternary catalyst that leads to a diminished amount of unwanted intermediates on the surface.

Regarding the Pt-RuO_2 binary coating, several reports in the literature by Rolison et al. [70–72] have shown that a mixed-phase electrocatalyst containing Pt and hydrous ruthenium oxides in the nanoscale size has an activity several orders of magnitude larger than metallic Pt-Ru alloys for methanol oxidation. Bulk quantities of electron–proton conduction by ruthenium oxides (rather than a near surface effect) are required to achieve high activity for methanol oxidation [70,71]. Thus, it was concluded [72] that hydrous ruthenium dioxide is a composite of anhydrous rutile-like RuO_2 nanocrystals dispersed by boundaries of structural water associated to Ru-O. Metallic conduction is supported by the rutile-like nanocrystals, while proton conduction is facilitated by the structural water along the grain boundaries. This structural picture could explain the electrocatalytic properties of $RuO_2 \cdot xH_2O$ in terms of competing percolation networks of metallic and protonic conduction pathways.

Moreover, the bi-functional mechanism [12] occurring in the ruthenium surface of Pt-Ru alloys is well-described in the literature [13] and is characterized by the formation of oxygenated species at low potentials that oxidize the CO_{ads} formed on the Pt surface. This effect seems to be enhanced by the effective initial presence of ruthenium oxides in the catalyst, as observed in the results shown in Fig. 8A and B for the binary coatings. There, the onset potentials for the alcohols oxidation reactions on RuO_2 modified electrodes are shifted to lower values and the cyclic voltammetric reactivation currents are smaller than those observed on the pure Pt catalyst. Consequently, the coatings containing RuO_2 show a better catalytic response for these reactions than pure platinum.

In the case of the Pt-RuO_2-RhO_2 ternary coating also presented in Fig. 8, the presence of RhO_2 renders an even better catalytic effect for those reactions by either promoting the oxidation of the adsorbed intermediates to CO_2 or weakening the adsorption of CO and other intermediates on the Pt surface for the composites coatings. Meanwhile, the specific role of Rh in alloy catalysts for the electrochemical oxidation of methanol is not fully understood and few examples are found in the literature.

Thus, Solymosi et al. [73] studied the adsorption and decomposition of methanol on metallic rhodium by electron energy loss and thermal desorption spectroscopy techniques and showed that methanol adsorbs readily on the Rh (1 1 1) surface at 100 K and that is effectively decomposed to adsorbed CO and H at 300 K. In addition, Williams et al. [74] studied the relationship between surface speciation and catalytic activity/selectivity during methanol oxidation on polycrystalline rhodium under ambient-pressure flow-reactor conditions by means of surface-enhanced Raman spectroscopy together with mass spectrometric measurements. They concluded that the strong catalytic properties of rhodium toward methanol oxidation appear to arise from the ability of adsorbed oxygen (and/or oxide) present at the surface to efficiently dissociate methanol and react with the resultant carbon-containing adsorbed fragments. This hallmark of rhodium is further highlighted by the presence of a CO_2 formation pathway via oxidation of adsorbed carbon produced by C–O bond scission.

Therefore, if it is assumed that the RhO_2 could shows similar properties and effects than metallic Rh, the better catalytic response observed on the Pt-RuO_2-RhO_2/BDD electrode (Fig. 8A) for the methanol oxidation reaction could be attributed to a facilitated adsorption and decomposition of the methanol molecule and to an increased tendency for the C–O bond scission on the RhO_2 surface. These effects, added to the others previously discussed for the presence of RuO_2 in the coating could explain the results in Fig. 8A.

On the other hand, Bergamaski et al. [75] studied the electrochemical oxidation of ethanol on Pt and Pt-Rh bimetallic electrodes prepared by potentiostatic deposition on a sputtered Au substrate by differential electrochemical mass spectroscopy (DEMS). These authors reported a good correlation between the extension of the dehydrogenation reaction at the beginning of the ethanol oxidation reaction and the production of CO_2 on Pt-Rh electrodes, revealing that a more extensive dehydrogenation destabilizes the ethanol molecule on the electrode surface

thus facilitating the C–C bond cleavage. Moreover, de Souza et al. [17] studied the electrochemical oxidation of ethanol using DEMS and in situ infrared spectroscopy (FTIR) techniques and reported that when Pt-Ru bimetallic electrodes are used the presence of Ru does not improve the CO_2 production over that of acetaldehyde but it was also observed that the presence of Rh in Pt-Rh bimetallic electrodes does effectively improve the CO_2 production. Thus, the addition of rhodium clearly increases the activity of the catalysts toward the C–C bond breaking, a fact not observed on Pt-Ru electrocatalysts.

Additionally, using DEMS experiments Iwasita and Pastor [76] and Silva-Chong et al. [77] reported that methane and ethane were observed during the further reduction of the poisoning adsorbates produced in the electro-oxidation of ethanol and acetaldehyde on metallic Pt electrodes. However, under the same experimental conditions only methane was detected on metallic Rh electrodes by Silva-Chong et al. [77] and Méndez et al. [78] who concluded that the Rh favors the deprotonation and cleavage of the C–C bond.

Therefore, making a correlation between the results presented above on materials with metallic Rh with those obtained in this study using RhO_2-containing electrodes in can be concluded that the earlier onset potential for the ethanol oxidation reaction observed on the Pt-RuO_2-RhO_2/BDD electrode (Fig. 9B) can probably be due to the ability shown by rhodium to promote C–C bond cleavage and deprotonation, added to the bifunctional effect of the Pt-Ru catalyst already mentioned.

Steady-state polarization curves as those shown in Fig. 9A and B are very useful tools for the study of the electrochemical oxidation of methanol and ethanol on the BBD modified electrodes. These measurements complemented, by the corresponding Tafel plots (insets in both figures), furnish a direct comparison of onset potentials and electrochemical activities in a straightforward manner. Data was obtained in the potentiostatic mode after 300 s polarization at each potential and it can be easily observed from those figures (Fig. 9A and B) that the best catalytic activity is obtained for the RhO_2-containing catalyst for both reactions under investigation.

The Tafel plots of Fig. 9A indicate that the methanol oxidation process starts at 0.48, 0.43 and 0.36 V versus HESS on Pt/BDD, Pt-RuO_2/BDD and Pt-RuO_2-RhO_2/BDD electrodes, respectively. The addition of RuO_2-RhO_2 to Pt/BDD produces a very active electrocatalyst lowering the onset potential in ~120 mV. It is worth mentioning that the observed onset potential on the Pt/BDD electrode (0.48 V) is in close agreement with those reported in the literature [53,56] for this electrode while it is lower than others measured for free-standing Pt anodes [79,80]. Furthermore, the 0.43 V versus HESS value of the onset potential for methanol oxidation observed on the Pt-RuO_2/BDD electrode is similar to that observed by Suffredini et al. [7,81] on Pt-RuO_2/C composites fixed on BBD and lower by approximately 0.5 V than the value reported by Tripković et al. [82] on Pt_2Ru_3 supported on carbon. In addition, the Pt-RuO_2-RhO_2/BDD electrode shows a less positive onset potential than those on Pt and Pt-Ru catalyst reported in the literature [7,53,56,79–82] while its catalytic activity is also better than the one recently reported by Park et al. [83] (0.45 V versus NHE) for a Pt-Ru-Rh-Ni (50:40:5:5) nanoparticle electrocatalyst. In addition, the stationary current density measured at a fixed potential of 0.57 V versus HESS is ca. five times larger for the Pt-RuO_2-RhO_2/BDD composite when compared to the Pt/BDD while the Pt-RuO_2/BDD catalyst is in between those values.

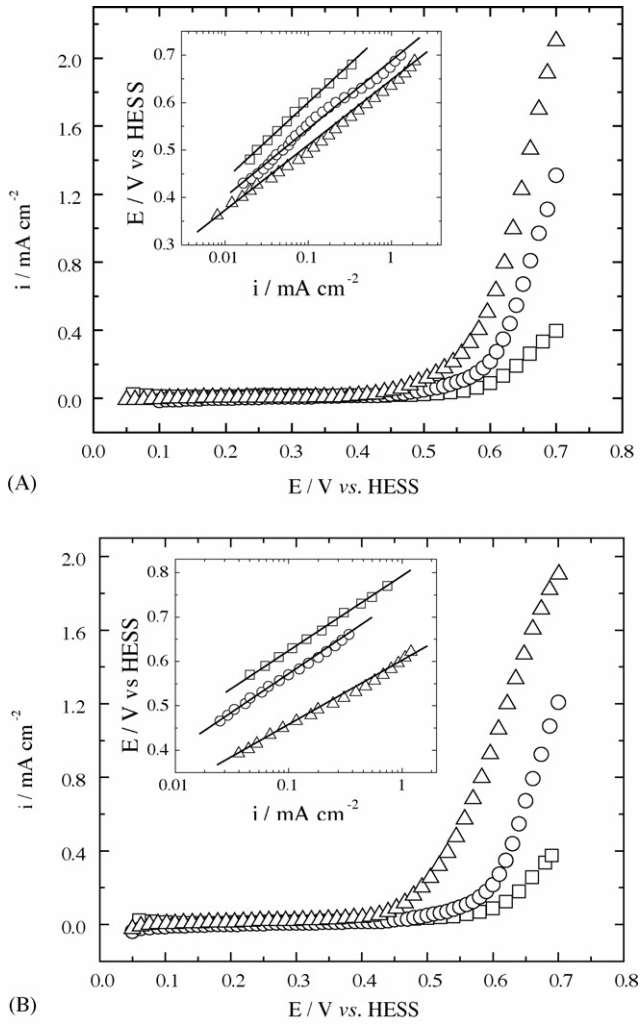

Fig. 9. Steady-state polarization curves for the electrochemical oxidation of 0.5 mol L^{-1} methanol (A) and 0.5 mol L^{-1} ethanol (B) dissolved in a 0.5 mol L^{-1} H_2SO_4 aqueous solution and recorded for the Pt/BDD (squares), Pt-RuO_2/BDD (spheres) and Pt-RuO_2-RhO_2/BDD (triangles) electrode surfaces. *Inset:* Tafel plots corresponding to each of the polarization curves.

Likewise, the onsets potential of ethanol oxidation reaction were in 0.57, 0.47, and 0.39 V versus HESS on Pt/BDD, Pt-RuO_2/BDD and Pt-RuO_2-RhO_2/BDD electrodes, respectively (inset of Fig. 9B). In this case, a lowering of 180 mV of the onset potential is observed for the Pt-RuO_2-RhO_2/BDD catalyst in comparison to Pt/BDD. Moreover, the value measured for this ternary composite on BDD (0.39 V) is ca. 100 mV lower than the best values previously reported for either Pt-Rh/PTFE (0.50 V) [17], Pt-Ru-Mo/C (0.45 V) [84], Pt-Rh bimetallic electrode (0.45 V) [75] or Pt-Os/Pt (1 1 1) single crystal (0.50–0.60 V) [85]. It is also important to note that the stationary current density determined at a fixed potential of 0.57 V versus HESS for the ethanol oxidation reaction (inset of Fig. 9B), is more

Table 3
Time and charge density passed before deviation from linearity (data from Fig. 10)

Electrode	Pt/C		Pt-RuO_2/C		Pt-RuO_2-RhO_2/C	
	Ethanol[a]	Methanol[a]	Ethanol[a]	Methanol[a]	Ethanol[a]	Methanol[a]
Time (s)	290	461	311	552	966	925
Charge density (mC cm^{-2})	41	82	90	117	370	258

[a] Alcohol.

than 12 times higher on Pt-RuO_2-RhO_2/BDD electrodes than on Pt/BDD while the Pt-RuO_2/BDD electrode appears in an intermediate position. This is a very important feature for catalysts to be used in practical applications.

Another important technique for the study of the surface stability of this type of electrocatalyst is the use of chronoamperometric measurement where the variation of the current density with time at a fixed potential could reveal poisoning effects. This can be achieved by observing negative deviations from Cottrell's law ($i \propto t^{-1/2}$) due to a blocking of the surface area in contrast to the normal positive deviations due to unwanted stirring of the solution. Moreover, a modification of that equation ($Q \propto t^{1/2}$) allows the determination of the amount of charge involved in the process for the different catalysts under investigation.

Fig. 10 shows the results obtained for the oxidation of methanol and ethanol at 0.55 V versus HESS on the Pt/BDD and Pt-RuO_2-RhO_2/BDD electrodes while Table 3 collects the results measured from the inset including now those intermediate values observed for the Pt-RuO_2/BDD composite. Apart from the fact that the current density in the ethanol oxidation reaction is 14.4 times higher for Pt-RuO_2-RhO_2 catalyst compared to Pt and the unexpected inversion of the sequence for the more active catalyst (i.e. larger current densities for ethanol oxidation), the curves at the inset of Fig. 10 and the values in Table 3 clearly indicate that the poisoning of the surface is much less intense for the ternary composite since the current follows

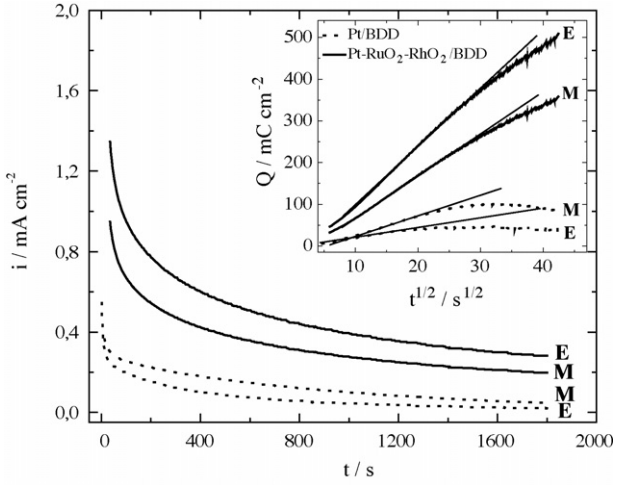

Fig. 10. Current density decays measured at a fixed potential of 0.55 V vs. HESS for the electrochemical oxidation of 0.5 mol L^{-1} methanol (M) and 0.5 mol L^{-1} ethanol (E) dissolved in a 0.5 mol L^{-1} H_2SO_4 aqueous solution and recorded for the Pt/BDD (dotted line) Pt-RuO_2-RhO_2/BDD (solid line) electrode surfaces. *Inset:* Charge density vs. $t^{1/2}$ plots for the same experiments.

the modified Cottrell's law for more than 16 min in a clear contrast to the 4–5 min observed on the Pt and Pt-RuO_2 catalysts.

These facts indicates that the addition of RuO_2 and RhO_2 to the Pt catalyst decreases the poisoning effect caused by the strongly adsorbed CO species generated during methanol oxidation and also improve the ethanol oxidation response, probably by facilitating the cleavage of the C–C bond of the adsorbed intermediate fragments. This is in qualitative agreement with the conclusions drawn from the cyclic voltammetric experiments but here those observations are properly quantified.

Finally, an important experimental observation is the fact that neither corrosion of the BDD support nor catalyst detachment or loss of the catalytic activity was detected during the experiments. This further demonstrate that the sol–gel modified surfaces have a high stability that is added to the extreme physical and chemical stability of the BBD support thus making these systems very promising candidates for anodes in fuel cells applications.

4. Conclusions

The physical characterization of the different composite materials deposited on BDD demonstrates that the relatively simple and low-cost sol–gel method is a very useful technique to modify BDD electrodes producing catalysts nanoparticles with a well controlled atomic composition and a homogeneous distribution on the surface.

Cyclic voltammograms for the methanol and ethanol oxidation reactions in acid media showed that the CO poisoning effect was largely inhibited on the composite electrode containing RhO_2, indicating the ability of the rhodium oxide to promote either the CO to CO_2 oxidation or a weaker adsorption of CO on the Pt neighboring atoms in the composite thus facilitating its subsequent removal.

Potentiostatic polarization curves for the methanol oxidation process revealed that the addition of RuO_2 and RhO_2 to the Pt/BDD composite produces a more reactive electrocatalyst that facilitates methanol adsorption shifting the reaction onset in 120 mV towards less positive potentials. This behavior could be due to a facilitated deprotonation of the methanol molecule on this surface in comparison to the Pt catalyst added to the bifunctional mechanism that usually predominates on Pt-Ru containing electrodes and even combined with the catalytic effect of the hydrous ruthenium dioxide.

Likewise, the ethanol oxidation reaction shows a decrease of 180 mV for the reaction onset on the Pt-RuO_2-RhO_2 catalyst in comparison to Pt. As a result of this earlier onset for the alcohol oxidation reaction, the stationary current density measured at a fixed potential increases considerably and becomes

over 12 times higher on Pt-RuO_2-RhO_2/BDD electrodes than on Pt/BDD and 7 times than on Pt-RuO_2/BDD electrodes. That earlier onset potential observed on the Pt-RuO_2-RhO_2/BDD electrode is probably due to the abilities shown by rhodium for the C–C bond cleavage and deprotonation, added to the bifunctional effect of the Pt-Ru catalyst.

Furthermore, chronoamperometric experiments analyzed by a modified Cottrell's law strongly suggest that poisoning of the surface by CO is greatly inhibited on the ternary composite electrode (Pt-RuO_2-RhO_2/BDD) if compared to the other two materials. Consequently, the current densities on that coating remain higher and diffusion-controlled for a considerable amount of time (or charge) thus making the catalyst containing Pt, RuO_2 and RhO_2 deposited on BDD by the sol–gel method a promising composite material to be used in fuel cell anodes.

Acknowledgements

The authors wish to thank to CAPES, CNPq and FAPESP (Proc. 01/14320-0), Brazil, for the scholarships and financial support to this work.

References

[1] H. Wendt, M. Gotz, M. Linardi, Tecnologia de Células a Combustível Química Nova 4 (2000) 538–546.
[2] A. Heinzel, V.M. Barragan, J. Power Sources 84 (1999) 70–74.
[3] E. Peled, T. Duvdevani, A. Aharon, A. Melman, Electrochem. Solid State Lett. 4 (2001) A38–A41.
[4] H.A. Gasteiger, N. Markovic, P.N. Ross, E.J. Cairns, J. Phys. Chem. 97 (1993) 12020–12029.
[5] Y. Morimoto, E.B. Yeager, J. Electroanal. Chem. 444 (1998) 95–100.
[6] L. Dubau, F. Hahn, C. Coutanceau, J.-M. Léger, C. Lamy, J. Electroanal. Chem. 554–555 (2003) 407–415.
[7] H.B. Suffredini, V. Tricoli, L.A. Avaca, N. Vatistas, Electrochem. Commun. 6 (2004) 1025–1028.
[8] T. Frelink, W. Visscher, J.A.R. Van Veen, Surf. Sci. 335 (1995) 353–360.
[9] C. Lamy, S. Rousseau, E.M. Belgsir, C. Coutanceau, J.-M. Léger, Electrochim. Acta 49 (2004) 3901–3908.
[10] F. Vigier, C. Coutanceau, F. Hahn, E.M. Belgsir, C. Lamy, J. Electroanal. Chem. 563 (2004) 81–89.
[11] H. Kita, H. Nakajima, K. Shimazu, J. Electroanal. Chem. 248 (1988) 181–191.
[12] M. Watanabe, S. Motoo, J. Electroanal. Chem. 60 (1975) 267–273.
[13] B.R. Gurau, R. Viswanathan, R.X. Liu, T.J. Lafrenz, K.L. Ley, E.S. Smotkin, E. Reddington, A. Sapienza, B.C. Chan, T.E. Mallouk, S. Sarangapani, J. Phys. Chem. B 102 (1998) 9997–10003.
[14] J.-M. Léger, S. Rousseau, C. Coutanceau, F. Hahn, C. Lamy, Electrochim. Acta 50 (2005) 5118–5125.
[15] M. Krausa, W. Vielstich, J. Electroanal. Chem. 379 (1994) 307–314.
[16] Y.Y. Tong, H.S. Kim, P.K. Babu, P. Waszczuk, A. Wieckowski, E. Oldfield, J. Am. Chem. Soc. 124 (2002) 468–473.
[17] J.P.I. de Souza, S.L. Queiroz, K. Bergamaski, E.R. Gonzalez, F.C. Nart, J. Phys. Chem. B 106 (2002) 9825–9830.
[18] S. Jayaraman, A.C. Hillier, Meas. Sci. Technol. 16 (2005) 5–13.
[19] L.M. Roen, C.H. Paik, T.D. Jarvi, Electrochem. Solid-State Lett. 7 (2004) A19–A22.
[20] C.H. Paik, T.D. Jarvi, W.E. O'Grady, Electrochem. Solid-State Lett. 7 (2004) A82–A84.
[21] K.H. Kangasniemi, D.A. Condit, T.D. Jarvi, J. Electrochem. Soc. 151 (2004) E125–E132.
[22] M. Hupert, A. Muck, J. Wang, J. Stotter, Z. Cvackova, S. Haymond, Y. Show, G.M. Swain, Diamond Relat. Mater. 12 (2003) 1940–1949.
[23] M. Uchida, Y. Aoyama, M. Tanabe, N. Yanagihara, N. Eda, A. Ohta, J. Electrochem. Soc. 142 (1995) 2572–2576.
[24] G.M. Swain, J. Electrochem. Soc. 141 (1994) 3382–3393.
[25] J. Wang, G.M. Swain, T. Tachibana, K. Kobashi, Electrochem. Solid State Lett. 3 (2000) 286–289.
[26] J. Wang, G.M. Swain, J. Electrochem. Soc. 150 (2003) E24–E32.
[27] E. Antolini, J. Mater. Sci. 38 (2003) 2995–3005.
[28] A.J. Appleby, Corrosion (Houston) 43 (1987) 398–408.
[29] G.M. Swain, A.B. Anderson, J.C. Angus, MRS Bull. 23 (1998) 56–60.
[30] Y.V. Pleskov, Russ. Chem. Rev. 68 (1999) 381–392 (Engl. Transl.).
[31] M.C. Granger, G.M. Swain, J. Electrochem. Soc. 146 (1999) 4551–4558.
[32] I. Duo, C. Lévy-Clément, A. Fujishima, C. Comninellis, J. Appl. Electrochem. 34 (2004) 935–943.
[33] H.B. Suffredini, V.A. Pedrosa, L. Codognoto, S.A.S. Machado, R.C. Rocha-Filho, L.A. Avaca, Electrochim. Acta 49 (2004) 4021–4026.
[34] G.R. Salazar-Banda, L.S. Andrade, P.A.P. Nascente, P.S. Pizani, R.C. Rocha-Filho, L.A. Avaca, Electrochim. Acta 51 (2006) 4612–4619.
[35] G.M. Swain, J. Electrochem. Soc. 141 (1994) 3382–3393.
[36] Q.Y. Chen, M.C. Granger, T.E. Lister, G.M. Swain, J. Electrochem. Soc. 144 (1997) 3806–3812.
[37] J. Iniesta, P.A. Michaud, M. Panizza, Ch. Comninellis, Electrochem. Commun. 3 (2001) 346–351.
[38] P.A. Michaud, E. Mahé, W. Haenni, A. Perret, Ch. Comninellis, Electrochem. Solid-State Lett. 3 (2000) 77–79.
[39] V.A. Pedrosa, L. Codognoto, L.A. Avaca, J. Braz. Chem. Soc. 14 (2003) 530–535.
[40] V.A. Pedrosa, L. Codognoto, S.A.S. Machado, L.A. Avaca, J. Electroanal. Chem. 573 (2004) 11–18.
[41] V.A. Pedrosa, H.B. Suffredini, L. Codognoto, S.T. Tanimoto, S.A.S. Machado, L.A. Avaca, Anal. Lett. 38 (2005) 1115–1125.
[42] L. Codognoto, S.A.S. Machado, L.A. Avaca, Diamond and Relat. Mater. 11 (2002) 1670–1675.
[43] G.W. Muna, N. Tasheva, G. Swain, Environ. Sci. Technol. 38 (2004) 3674–3682.
[44] C.E. Banks, M.E. Hyde, P. Tomcik, R. Jacobs, R.G. Comptom, Talanta 62 (2004) 279–286.
[45] M. Panizza, P.A. Michaud, G. Cerisola, Ch. Comninellis, J. Electroanal. Chem. 507 (2001) 206–214.
[46] I. Troster, M. Fryda, D. Herrmann, L. Schafer, W. Hanni, A. Perret, M. Blaschk, A. Kraft, M. Stadelmann, Diamond Relat. Mater. 11 (2002) 640–645.
[47] L. Codognoto, S.A.S. Machado, L.A. Avaca, J. Appl. Electrochem. 33 (2003) 951–957.
[48] E. Brillas, B. Boye, I. Sires, J.A. Garrido, R.M. Rodriguez, C. Arias, P.L. Cabot, C. Comninellis, Electrochim. Acta 49 (2004) 4487–4496.
[49] J.F. Zhi, H.B. Wang, T. Nakashima, T.N. Rao, A. Fujishima, J. Phys. Chem. B 107 (2003) 13389–13395.
[50] R. Bellagamba, P.A. Michaud, C. Comninellis, N. Vatistas, Electrochem. Commun. 4 (2002) 171–176.
[51] A.E. Fischer, G.M. Swain, J. Electrochem. Soc. 152 (2005) B369–B375.
[52] M. Awada, J.W. Strojek, G.M. Swain, J. Electrochem. Soc. 142 (1995) L42–L45.
[53] F. Montilla, E. Morallon, I. Duo, C. Comninellis, J.L. Vazquez, Electrochim. Acta 48 (2003) 3891–3897.
[54] G.R. Salazar-Banda, H.B. Suffredini, L.A. Avaca, J. Braz. Chem. Soc. 16 (2005) 903–906.
[55] H.B. Suffredini, G.R. Salazar-Banda, S.T. Tanimoto, M.L. Calegaro, S.A.S. Machado, L.A. Avaca, J. Braz. Chem. Soc. 16 (2006) 257–264.
[56] K. Honda, M. Yoshimura, T.N. Rao, D.A. Tryk, A. Fujishima, K. Yasui, Y. Sakamoto, K. Nishio, H. Masuda, J. Electroanal. Chem. 514 (2001) 35–50.
[57] A. Trinchi, Y.X. Li, W. Wlodarski, S. Kaciulis, S. Pandolfi, S.P. Russo, J. Duplessis, S. Viticoli, Sens. Actuators A: Phys. 108 (2003) 263–270.
[58] F. Perdomo, L.P. de Lima-Neto, M.A. Aegerter, L.A. Avaca, J. Sol–Gel Sci. Technol. 15 (1999) 87–91.
[59] F.I. Mattos-Costa, P. de Lima-Neto, S.A.S. Machado, L.A. Avaca, Electrochim. Acta 44 (1998) 1515–1523.

[60] H.B. Suffredini, J.L. Cerne, F.C. Crnkovic, S.A.S. Machado, L.A. Avaca, Int. J. Hydrogen Energy 25 (2000) 415–423.
[61] M.S. Loffler, H. Natter, R. Hempelmann, K. Wippermann, Electrochim. Acta 48 (2003) 3047–3051.
[62] J. Prabhuram, T.S. Zhao, C.W. Wong, J.W. Guo, J. Power Sources 134 (2004) 1–6.
[63] T.C. Deivaraj, W. Chen, J.Y. Lee, J. Mater. Chem. 13 (2003) 2555–2560.
[64] J. Pagnaer, D. Nelis, D. Mondelaers, G. Vanhoyland, J. D'Haen, M.K. Van Bael, H. Van den Rul, J. Mullens, L.C. Van Poucke, J. Eur. Ceram. Soc. 24 (2004) 919–923.
[65] S. Krumm, Comp. Geosci. 25 (1999) 489–499.
[66] N.G. Ferreira, L.L.G. Silva, E.J. Corat, V.J. Trava-Airoldi, Diamond Relat. Mater. 11 (2002) 1523–1531.
[67] C.H. Goeting, F. Jones, J.S. Foord, J.C. Eklund, F. Marken, R.G. Compton, P.R. Chalker, C. Johnston, J. Electroanal. Chem. 442 (1998) 207–216.
[68] H.B. Suffredini, S.A.S. Machado, L.A. Avaca, J. Braz. Chem. Soc. 15 (2004) 16–21.
[69] R.T.S. Oliveira, M.C. Santos, B.G. Marcussi, P.A.P. Nascente, L.O.S. Bulhões, E.C. Pereira, J. Electroanal. Chem. 575 (2005) 177–182.
[70] D.R. Rolison, P.L. Hagans, K.E. Swider, J.W. Long, Langmuir 15 (1999) 774–779.
[71] J.W. Long, R.M. Stroud, K.E. Swider-Lyons, D.R. Rolison, J. Phys. Chem. B 104 (2000) 9772–9776.
[72] W. Dmowski, T. Egami, K.E. Swider-Lyons, C.T. Love, D.R. Rolison, J. Phys. Chem. B 106 (2002) 12677–12683.
[73] F. Solymosi, A. Berkó, T.I. Tarnóczi, Surf. Sci. 141 (1984) 533–548.
[74] C.T. Williams, C.G. Takoudis, M.J. Weaver, J. Phys. Chem. B 102 (1998) 406–416.
[75] K. Bergamaski, J.F. Gomes, B.E. Goi, F.C. Nart, Eclética Quím. 28 (2003) 87–92.
[76] T. Iwasita, E. Pastor, Electrochim. Acta 39 (1994) 531–537.
[77] J.A. Silva-Chong, E. Méndez, C. Arévalo, J.L. Rodríguez, E. Pastor, Electrochim. Acta 47 (2002) 1441–1449.
[78] E. Méndez, J.L. Rodríguez, C. Arévalo, E. Pastor, Langmuir 18 (2002) 763–772.
[79] S.Lj. Gojković, T.R. Vidaković, Electrochim. Acta 47 (2001) 633–642.
[80] T. Iwasita, Electrochim. Acta 47 (2002) 3663–3674.
[81] H.B. Suffredini, V. Tricoli, N. Vatistas, L.A. Avaca, J. Power Sources 158 (2006) 124–128.
[82] A.V. Tripković, K.D. Popović, B.N. Grgur, B. Blizanac, P.N. Ross, N.M. Marković, Electrochim. Acta 47 (2002) 3707–3714.
[83] K.-W. Park, J.-H. Choi, S.-S. Lee, C. Pak, H. Chang, Y.-E. Sung, J. Catal. 224 (2004) 236–242.
[84] A. Oliveira Neto, E.G. Franco, E. Aricó, M. Linardi, E.R. Gonzalez, J. Eur. Ceram. Soc. 23 (2003) 2987–2992.
[85] V. Pacheco Santos, V. Del Colle, R. Batista de Lima, G. Tremiliosi-Filho, Langmuir 20 (2004) 11064–11072.